JCTC Journal of Chemical Theory and Computation

pubs.acs.org/JCTC Article

Using Density-Corrected DFT to Understand Density-Driven and Functional-Dependent Errors in Ab Initio Simulations of the Hydrated Electron

William R. Borrelli, José L. Guardado Sandoval, and Benjamin J. Schwartz*

Cite This: J. Chem. Theory Comput. 2026, 22, 2550−2561 Read Online

ACCESS | Metrics & More | Article Recommendations | Supporting Information

ABSTRACT: The hydrated electron, an excess electron in liquid water, plays a crucial role in a plethora of chemical processes, motivating extensive research efforts to characterize its structure, dynamics, and reactivity in solution. Recent theoretical approaches to understanding this intriguing object have involved ab initio simulations based on density functional theory (DFT). Although DFT allows for the study of hydrated electron reactivity and quantum mechanical behavior, it is well-known that anionic systems can suffer from significant density-driven errors (DDEs). Density-corrected DFT (DC-DFT) provides a framework to mitigate such errors; the method reduces DDEs by replacing the self-consistent (SC) density associated with a given density functional with the Hartree−Fock (HF) density. Since HF densities tend to be more localized than DFT SC densities, the DC-DFT scheme significantly improves errors in calculations where the SC density is spuriously delocalized. Here, we investigate how the use of density correction affects the calculated properties of the DFT-simulated (PBEh) hydrated electron, a particularly challenging diffuse anionic system to simulate. First, we analyze charge delocalization in a system consisting of a model octahedral hydrated electron water cluster (the so-called Kevan structure) along with a spatially separated sulfur atom. We show that the use of density correction indeed reduces DDEs in comparison to a standard DFT global hybrid functional. We then propagate molecular dynamics trajectories of the hydrated electron using DC-DFT, where we find that DC further localizes electron density in the cavity region, a signature of reduced charge delocalization. Unfortunately, the decreased radius of gyration of the spin density and corresponding tightening of the local solvation structure from density correction causes predicted observables to deviate further from experimental measurements than when density correction is not employed. We argue that DC's worse agreement with experiment results from the removal of a fortuitous cancellation of errors that is intrinsic to the PBEh functional. This indicates that the difficulties with DFT to simulate hydrated electrons are primarily due to the inherent approximations in DFT rather than to density-driven errors.

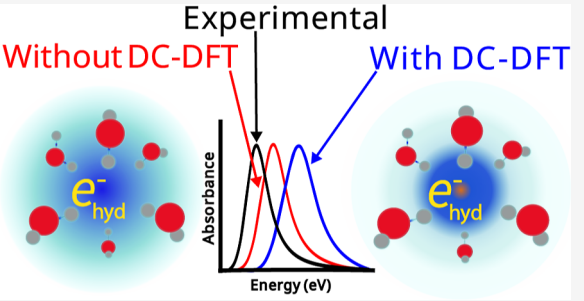

INTRODUCTION

Hydrated electrons, chemical species formed when excess electrons become solvated in aqueous environments, are highly reactive anions that drive numerous chemical processes. These fundamental yet complex species are of particular significance in radiation chemistry,[1−6] serve as important probes for understanding interfacial water chemistry,[7−11] and contribute to biological damage through indirect DNA modification pathways.[12−14] As a result, there has been particular interest in simulating the properties and reactivity of hydrated electrons. Experimental and theoretical work largely agree that the electron occupies a quasi-spherical cavity, where water molecules stabilize the electron cavity via a H-bonding motif.[15−17] However, there still is no consensus on other details of the solvation structure, such as the local degree of solvent ordering or the nature of the equilibrium solvent fluctuations, which are crucial for understanding the behavior, reactivity, and spectroscopy of the hydrated electron.

Although most simulation models of the hydrated electron predict a H-bonded cavity structure, these models differ substantially in how they predict experimental observables.[16,18−21] For the last several decades, most hydrated electron simulations have used mixed quantum-classical (MQC) molecular dynamics (MD) methodologies, where the solvent is treated classically and the single excess electron is treated quantum mechanically.[22−24] The electron-water interaction is described by a pseudopotential,[21,25−27] which is a potential function that is usually parametrized from ab initio calculations. MQC models have the advantage of being computationally efficient, allowing such simulations to contain

Received: November 20, 2025
Revised: February 3, 2026
Accepted: February 6, 2026
Published: February 23, 2026

https://doi.org/10.1021/acs.jctc.5c01944
J. Chem. Theory Comput. 2026, 22, 2550−2561

hundreds or thousands of water molecules and achieve simulation times of nanoseconds. Unfortunately, however, results from this level of theory depend heavily on the choice of the pseudopotential.[21,27−31] Different pseudopotential models show varying performance in their predictions of experimental observables,[32−34] with no single model proving to be superior across the board. The classical description of the solvent also makes the simulation of reactive chemistry impossible with this methodology.

Recently, with advances in computational resources, density functional theory (DFT) has emerged as a potentially tractable ab initio method for hydrated electron simulations of moderate size and trajectory length. Moreover, the fact that DFT treats all parts of the system quantum mechanically means that one can directly simulate reactive chemistry. As a result, there has been a significant amount of work applying DFT-based simulations to hydrated electron systems, simulating this object to investigate its solvation,[16,19,35,36] spectroscopy,[8,35,37−41] and reactivity.[20,42−44] Less well explored, however, is whether or not DFT (or at least particular exchange−correlation functionals)[16] provides an adequate level of theory for describing hydrated electrons, which is the focus of the current work.

One of the challenges of using DFT to simulate hydrated electrons is that they necessarily exist only in aqueous solution, meaning that a faithful description of liquid water is necessary to simulate these objects. Historically, reproducing the experimental properties of liquid water with DFT has been a challenge, largely because of the need to accurately model both the strong covalent interactions in water's O−H bonds as well as the weaker noncovalent interactions that dominate hydrogen bonding.[45,46] It is only recently that global hybrid generalized gradient approximation (GGA) density functional approximations (DFAs) with dispersion corrections (such as PBEh-D3) and meta-GGA functionals (such as the SCAN functionals) have been shown to model bulk water with high accuracy.[45,47,48] However, there has been comparably little work using such DFAs to simulate hydrated electrons, and the little work that has been done found that many of the functionals that have been tested do not even predict that a localized hydrated electron exists.[16,18,49] Simpler DFAs not only do not describe liquid water well, but the DFT-based hydrated electron tends to form a more rigid and structured solvation environment with a smaller central cavity compared to MQC models. DFT hydrated electron simulations also have shown mixed performance in predicting experimental observables.[16,18,31,33,50,51]

Yet another obstacle with using DFT to simulate hydrated electrons is contending with density-driven errors (DDEs), which can often result in excess charge delocalization due to self-interaction error (SIE). It is widely known that when approximate DFAs are applied to one-electron systems, the exchange energy does not exactly cancel the Coulomb energy.[52] This leads to a spurious interaction of an electron with itself, which can manifest as an unphysical overdelocalization of charge. In fact, the fractional charge behavior displayed by many DFAs is often used as a way of examining SIE.[52] SIE is known to be particularly prevalent in simulations of solution-phase anions,[53] and the hydrated electron is a particularly challenging anion to simulate because it lacks an attractive binding force from a nucleus. In past work, we posited that delocalization error could be inducing the highly structured solvation motifs exhibited by DFT-simulated hydrated electrons,[16,19,35,38,41] but to date there have been no studies investigating the source of possible errors with DFT simulations of this object.

All of this leads to the question that is the focus of this work: to what extent do density-driven versus functional errors impact DFT-based simulations of the hydrated electron? We attack this problem by using density-corrected DFT (DC-DFT),[53,54] which is a calculation framework that can help to separate the errors made by approximate DFAs into density-driven and functional-dominated errors.[53,55] This method has been shown to reduce DDEs in a variety of systems, including anionic water clusters.[55−60] DC-DFT is based on using the Hartree−Fock (HF) rather than the self-consistent density when the system is deemed density sensitive; this means that DC-DFT avoids excess charge delocalization in cases in which the self-consistent density is abnormally delocalized. Here, using reference calculations based on a symmetric model hydrated electron system,[61] we show that DC-DFT does adequately correct for the DDEs present in DFT calculations of an excess electron bound by surrounding water molecules. We then run a 64-water ab initio hydrated electron simulation using DC-DFT with a global hybrid functional (PBEh) with two different amounts of exact exchange (25% and 40%); our hope was that the use of the DC methodology would lead to significant improvements in the properties of the resultant simulated hydrated electron due to an attenuation of DDEs.

What we found, however, is that despite reducing DDEs, the experimental observables predicted by DC-DFT hydrated electron simulations are actually in worse agreement with experiment than simulations without density correction. In particular, we see that density correction causes further structuring of the electron-water radial and angular distributions, which even without density correction are already far more structured for DFT than for MQC models. This causes the DC-DFT-simulated electron's radius of gyration (R_g) and vertical binding energy (VBE) to decrease, thus moving farther from the experimentally determined values[15,62−67] than for simulations without density correction. The use of DC-DFT also worsens the predicted shape of the absorption spectrum relative to experiment. An error decomposition analysis shows that DC worsens a fortuitous DFT cancellation of errors, so that functional-driven errors remain the dominant error source for PBEh-based calculations on hydrated electron systems, in line with previous work.[68] All of the results indicate that although density-related errors are present in DFT-based simulations of the hydrated electron, these errors are not the primary factor causing disagreement between DFT-based simulation predictions and experimental results.

RESULTS AND DISCUSSION

The fact that DFT-based hydrated electron simulations are prone to DDEs has been known since the earliest such simulations performed by Uhlig et al.[51] These workers used a QM/MM scheme with the BLYP functional[69−71] but found that a self-interaction correction[72] was necessary to form a localized hydrated electron; without this correction, the electron delocalized across the entire simulation cell due to errors associated with the BLYP DFA. More recent work has established that some hybrid functionals, such as PBEh,[73] do form localized hydrated electrons, although we recently have shown that other DFAs, including some meta-GGA hybrid functionals that are expected to have reduced DDEs, do not.[16] It is worth noting that the explicit inclusion of Hartree−Fock

https://doi.org/10.1021/acs.jctc.5c01944
J. Chem. Theory Comput. 2026, 22, 2550−2561

Table 1. Charge Analysis for the Sulfur (q_s) and Ghost Atom (q_{Gh}) from "Combined" Kevan−Ghost−Sulfur Systems (Either the Idealized Kevan Structure, Left Column, or the First Solvation Shell Taken from Ab Initio DC-DFT MD Simulations, Right Column) and Density Sensitivity Assessment ($\tilde{S}$, Equation 2) of the Kevan/First-Shell Structure across Different Levels of Theory

	Kevan			first shell		
functional/method	q_S (e)	q_{Gh} (e)	$\tilde{S}$ (kcal/mol)	q_S (e)	q_{Gh} (e)	$\tilde{S}$ (kcal/mol)
PBEh(25%)-D3	−0.62	−0.60	2.8	−0.72 ± 0.03	−0.18 ± 0.04	4.1 ± 1.3
PBEh(40%)-D3	−0.68	−0.51	13.5	−0.85 ± 0.02	−0.18 ± 0.12	7.8 ± 1.3
DC-PBEh(25%)-D3	−1.0	−0.19	-	−1.0	−0.13 ± 0.13	-
DC-PBEh(40%)-D3	−1.0	−0.19	-	−1.0	0.05 ± 0.04	-
LRC-ωPBE	−1.0	−0.13	-	-	-	-
HF	−1.0	−0.19	-	-	-	-

(HF) exchange in hybrid DFAs helps to localize charge densities and reduce DDEs. However, global hybrid functionals still suffer from density-driven error as well as incorrect asymptotic behavior of the exchange−correlation potential at long distances.[74] Here, we aim to understand these limitations through the DC-DFT framework.

As an approach to understanding charge delocalization, density-corrected DFT was formulated to separate the errors made by using approximate DFAs into errors in the self-consistent (SC) density (density-driven errors) and errors resulting from the functional itself (functional-dominant contribution).[53] DC-DFT reduces the delocalization error of DFAs by replacing the SC density (which can be prone to SIE and other density-driven errors) with the HF density (which is free from SIE and, thus, generally more localized than the SC density). In other words, the HF density is taken to be a closer approximation to the true density than the SC density. This approach has been demonstrated to effectively mitigate errors arising from electron delocalization in a wide array of systems, including those involving torsional barriers,[59] solution-phase radicals,[58] aqueous anions,[55−60] and complexes with halogen bonds.[75]

Here, we apply DC-DFT to better understand how pervasive delocalization error is for DFT-simulated hydrated electron systems. We find that although DC successfully reduces charge delocalization, it worsens agreement with experimental observables compared with standard PBEh functionals. Our simulations reveal that DC produces quantitative changes in predicted hydrated electron observables without qualitative differences in the electron-water solvation structure. We also perform an energy decomposition analysis, which suggests that the introduction of DC actually worsens fortuitous cancellation of errors. These findings indicate that innate functional limitations, rather than density-driven errors, represent the primary source of inaccuracy in hydrated electron simulations that cannot be resolved with DC alone.

Quantifying DDEs for the DFT-Simulated Hydrated Electron

To quantify the degree of delocalization error present in DFT-based calculations, a well-known measure is examining the degree of convex curvature of the total energy as a function of the number of electrons in the system, $E(N)$. If the exact exchange−correlation functional was known, $E(N)$ would be piece-wise linear and have derivative discontinuities at the integer charge states.[76] For typical DFAs, however, $E(N)$ tends to be convex, leading to the commonly seen DFT overestimation of the electron affinity and underestimation of the ionization energy.[77]

To determine whether or not DC-DFT can alleviate the DDEs associated with the PBEh DFA, which is what is most commonly used for DFT-based simulations of the hydrated electron,[16,36,38,78] we turn to a type of $E(N)$ analysis inspired by Johnson and co-workers.[61,79] Their idea is to test for spurious charge delocalization by constructing an anionic system containing two fragments that can bind an electron that are separated by a large distance. A functional or level of theory that does not suffer from DDE should localize all of the excess charge onto the fragment with the greater electron affinity; a DFA that is subject to DDE will delocalize the charge over both fragments.

Following Johnson and co-workers,[61,79] we constructed an anionic system using a minimalistic model of the hydrated electron known as the Kevan structure,[38,80] which contains six water molecules octahedrally arranged around a central cavity with one water O−H bond pointing directly toward the cavity center. We then placed a sulfur atom 20 Å away from the center of the Kevan cluster and calculated the partial charges of each atom in the system. For calculation purposes, we placed a ghost atom at the center of the Kevan cluster to better capture excess electron charge in the cavity region.[41,61] We refer to this Kevan cluster plus separated S atom construction as the "combined" system.

For the combined system, at most levels of theory, the S atom has an electron affinity that is several eV greater than that of the Kevan structure. This means that an excess electron added to the combined system should localize entirely on the S atom in the absence of DDE. We performed calculations on the combined system at several levels of theory, including using the PBEh global hybrid functional with both 25% and 40% exact exchange and D3 dispersion,[71] which is what is most commonly used for DFT-based hydrated electron simulations.[19,20,44,81] We note that these two amounts of exact exchange were chosen because (a) 25% is the "default" amount of exact exchange for the PBE0 functional and (b) 40% exact exchange was empirically found to optimize the prediction of the band gap of liquid water.[82] In addition to PBEh, we also explored using a range-separated hybrid functional (LRC-ωPBE) as well as Hartree−Fock (HF). We show in the Supporting Information that all of the results presented here hold true regardless of the inclusion/exclusion of the D3 dispersion correction[71] and are also independent of the use of D4[83] dispersion or a density-consistent dispersion parametrization.[84] This makes physical sense, as the addition of a classical dispersion correction does not alter the density.

The "Kevan" column in Table 1 shows the computed Mulliken charges (in fraction of an electron charge) both on the S atom (q_S) and on the ghost atom in the cavity of the

https://doi.org/10.1021/acs.jctc.5c01944
J. Chem. Theory Comput. 2026, 22, 2550−2561

Kevan cluster (q_{Gh}) for the anion of the combined system at each level of theory. The results indicate that PBEh with both 25% and 40% HF exchange is subject to DDE, as the charge on the S atom is not −1.0 e. Instead, charge is distributed partially on the sulfur atom and partially on the ghost atom and water molecules of the Kevan cluster. Both density-corrected versions of these functionals, as well as the range-separated hybrid DFA and HF, give the S atom a charge of −1.0 e, indicating the correct localization behavior and thus the absence of DDE.

To further investigate the charge delocalization behavior, we calculated $E(N)$ curves for charging of the Kevan cluster alone. This was accomplished by completing fractional charge calculations at a number of discrete charge values ranging from 0 (neutral cluster) to −1 (anionic cluster). In the Supporting Information, we also test an interpolation scheme proposed by Johnson and co-workers[61] that can recover energy values at fractional charge occupations using the energies obtained from calculations of only the fully neutral and anionic systems; we find that this interpolation scheme works extremely well for the non-DC functionals and qualitatively well for the DC functionals. The data presented below, however, are for our explicit fractional charge calculations.

We also note that $E(N)$ curves are typically constructed for calculations where the functional used to calculate the energy is also the source of the electron density. DC-DFT differs in this regard, as the density comes from HF theory, while the energy is calculated using a DFA. Although this can potentially complicate the analysis of $E(N)$ curves for DC functionals, piece-wise linearity of the $E(N)$ curve is a fundamental requirement regardless of the source of the densities or energies used to construct it, so examining the curvature of such plots for density-corrected functionals still makes sense.

The solid curves in Figure 1 panels (a−c) show the $E(N)$ charging plots for the Kevan structure for each functional/level of theory; the various dashed lines show the exact ideal linear behavior. It is clear that PBEh(25%) is subject to DDEs given the convexity of the red curve in panel (a) and that the DDEs are reduced with the addition of more HF exchange, causing the orange PBEh(40%) curve to become less convex. Panel (c) shows that the range-separated LRC-ωPBE functional (green curve) as well as HF theory (cyan curve) give concave curves. Panel (b) shows that the density-corrected PBEh functionals show slightly concave behavior, very close to the ideal linear trend. This analysis fits well with our findings from the combined system: the levels of theory that give concave $E(N)$ curves (HF, LRC-ωPBE, and DC-PBEh) yield the correct localization behavior and result in a partial charge of −1 e on the S atom, while the PBEh functionals that give convex curves result in only a partial charge on the combined-system S atom. We also calculated charge-transfer curves, similar to those presented by Johnson and co-workers,[61] plotting the energy as charge is moved from the Kevan structure to the distant sulfur atom, which are shown in the Supporting Information.

Another way to determine whether density correction can improve the results for a given DFT system is to calculate a measure of density sensitivity. Several groups have introduced density sensitivity measures,[85−87] but here we focus on $\tilde{S}$, developed by Burke and co-workers, which is defined as[53]

$$\tilde{S} = |\tilde{E}[n^{HF}] - \tilde{E}[n^{LDA}]| \quad (1)$$

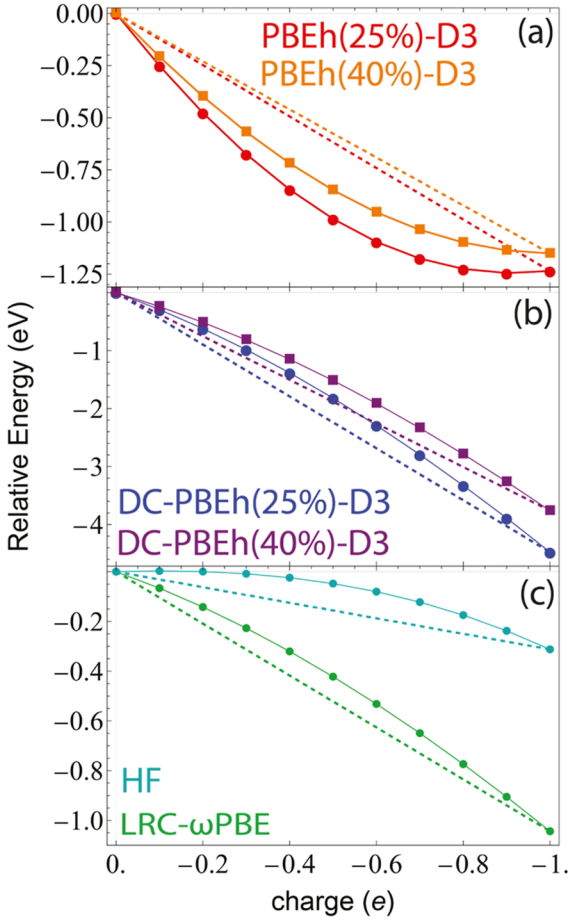

Figure 1. (a−c) Explicitly calculated $E(N)$ plots for the Kevan structure, following Johnson and co-workers,[61] computed with various levels of theory. In all panels, the dashed lines represent the ideal linear behavior corresponding to no charge delocalization. Convex curvature indicates charge delocalization error, while concave curvature reflects overlocalization. (a) PBEh with 25% HF exchange (red curve) and 40% HF exchange (orange curve). Increasing HF exchange reduces the convexity of the charging curve, diminishing the minimum at fractional charge values and thereby improving charge delocalization. (b) DC-PBEh with 25% HF (navy) and 40% HF (purple) show slightly concave behavior, indicating a reduction of DDEs, as well as a much lower binding energy. (c) LRC-ωPBE (green) and pure HF (cyan) both exhibit concave curves characteristic of overlocalization, with LRC-ωPBE approaching the ideal linear behavior more closely than HF. Each point is a fractional charge calculation, with the connecting line segments to guide the eye.

where n^{HF} is the Hartree−Fock density, n^{LDA} is the LDA SC density, and $\tilde{E}[n]$ is the energy evaluated with a given DFA using density n^i. Previous work[53] has argued that $\tilde{S} \geq \sim 2.0$ kcal/mol (although larger cutoff values have been used for larger systems[60]) means that a system is density sensitive with a given DFA. Table 1 shows values of $\tilde{S}$ calculated for the anion of the Kevan structure using PBEh(25% and 40%). With either amount of HF exchange, it is clear that the use of PBEh for hydrated electron simulations, and particularly PBEh(40%), is density sensitive.

Using Density-Corrected DFT to Simulate the Bulk Hydrated Electron

Given that DC appears to successfully address DDE in minimal hydrated electron models, we performed ab initio MD

https://doi.org/10.1021/acs.jctc.5c01944
J. Chem. Theory Comput. 2026, 22, 2550−2561

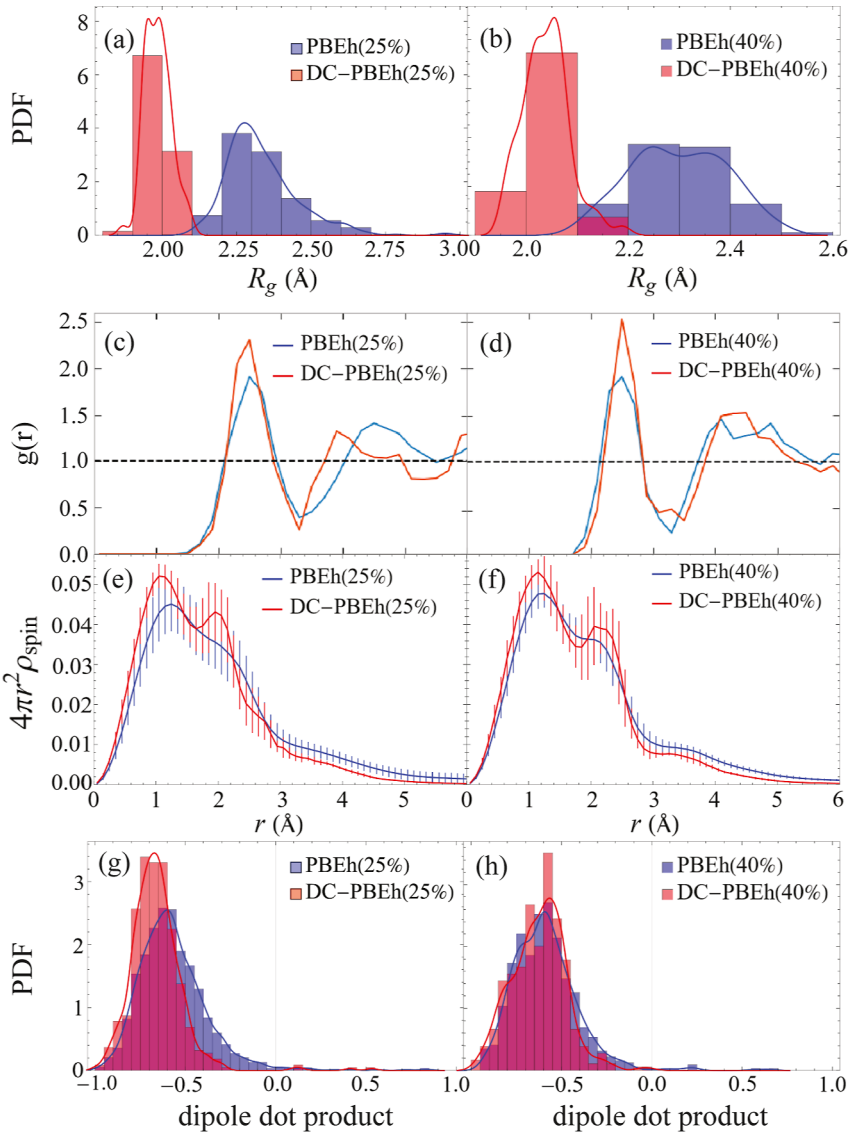

Figure 2. Comparison of 64-water DFT-simulated bulk hydrated electron properties using standard and density-corrected PBEh functionals with D3 dispersion.[71] The left panels compare PBEh(25%)-D3 (blue) with DC-PBEh(25%)-D3 (orange), while the right panels compare PBEh(40%)-D3 (blue) with DC-PBEh(40%)-D3 (orange). (a,b) Radius of gyration distributions for the bulk hydrated electron. The application of DC reduces the electron's radius of gyration for both PBEh-D3 functionals, indicating decreased electron delocalization. (c,d) Electron-water radial distribution functions are largely unaffected by the use of DC, despite the observed differences in gyration radii. DC does lead to a slight tightening of the first solvation shell. (e,f) Charge density distributions show that DC redistributes hydrated electron density by removing charge that extends past the first solvation shell and concentrating it on the first-shell waters and within the cavity, consistent with the R_g changes observed in a and b. (g,h) Angular distribution of the first-shell waters around the hydrated electron, calculated as a dot product between a vector connecting the electron's spin density center of mass and a first-shell water O atom and that water's dipole vector. Values near −0.7 indicate H-bond solvation of the electron. DC enhances the electron-water structural ordering, with the effect being more pronounced for PBEh(25%)-D3.

simulations using the DC-PBEh(25%) and DC-PBEh(40%) levels of theory, both with the D3 dispersion correction.[71] The simulations employed periodic boundary conditions with 64 water molecules and one excess electron. The DC simulations were initialized from equilibrated configurations of the corresponding standard PBEh trajectories from our previously published work[16,38] and all simulation parameters were kept identical, allowing for direct comparison of hydrated electron properties between the density-corrected and uncorrected functionals. The computational overhead associated with density correction increased time step costs by approximately 3-fold, limiting DC trajectory lengths to ∼5 ps compared to the ∼20 ps durations for PBEh(25%) in our previous work.

Figure 2 summarizes the results of our DC-DFT simulations of the bulk hydrated electron. Panels a and b show the distribution of the electron's radius of gyration (calculated from the spin density), panels c and d show the electron-water radial distribution functions, and panels e and f show the spin density distributions. The left panels compare the results for PBEh(25%) (blue) and DC-PBEh(25%) (orange), while the right panels compare PBEh(40%) (blue) and DC-PBEh(40%) (orange), and panels g and h show angular distributions of the first-shell water molecules around the electron.

The results show that the most dramatic difference that comes from the use of density correction is in the excess electron's radius of gyration, (R_g), where DC leads to a ∼15%

https://doi.org/10.1021/acs.jctc.5c01944
J. Chem. Theory Comput. 2026, 22, 2550−2561

Table 2. Bulk Simulated Hydrated Electron Radius of Gyration, R_g (Å) (with Uncertainties Given as the Raw Standard Deviations), Absorption Spectrum E_{max} (eV), VBE (eV) (with Uncertainties Given as the Raw Standard Deviations), and V_M (cm^3/mol) (with Uncertainties from Bootstrapping Analysis) for PBEh(25% and 40%)-D3 with and without DC, as Well as Experimental Values

functional/method	R_g (Å)	absorption E_{max} (eV)	VBE (eV)	V_M (cm^3/mol)
PBEh(25%)-D3	2.33 ± 0.12	2.5	2.14 ± 0.36	8.0 ± 3.1
PBEh(40%)-D3	2.30 ± 0.10	2.2	1.78 ± 0.26	8.3 ± 2.9
DC-PBEh(25%)-D3	1.99 ± 0.04	2.6	1.76 ± 0.21	5.5 ± 2.5
DC-PBEh(40%)-D3	2.04 ± 0.05	2.2	1.70 ± 0.40	9.0 ± 2.6
experiment	2.45[67]	1.73[66]	3.5[15,64,65]	26 ± 6[62,63]

reduction in the size of the hydrated electron's charge density. This result makes sense given that HF densities are more localized than SC densities.[52,53,88] This result also agrees with our previous study on the DFA dependence of DFT-simulated hydrated electrons, which found that hybrid meta-GGA DFAs, which should have reduced DDEs, generally produced smaller hydrated electrons than hybrid GGA DFAs, although the magnitude of the difference was not as large as we see here with DC.[16] Unfortunately, however, the smaller $R_g \approx 2.0$ Å values predicted with DC are actually in worse agreement with the experimental radius of gyration of 2.45 Å, obtained by spectral moment analysis,[67] than the larger values obtained without DC.

The radial distribution functions (RDFs) in Figure 2c,d show that the distances at which water molecules prefer to sit away from the electron cavity do not undergo much change with the use of DC, despite the fact that the electron's radius of gyration is significantly smaller for the DC functionals. DC does produce a small enhancement of the first-shell peak, which likely results from increased charge density in the cavity and on the first-shell waters due to greater localization of the HF density compared with the SC density. The net result is that the use of DC slightly increases the translational ordering of the water molecules around the hydrated electron.

The RDFs in Figure 2c,d are directly connected to the hydrated electron's molar solvation volume, V_M, which is an experimental observable.[62,63] V_M can be calculated from an integral of the RDF via the Kirkwood−Buff (KB) formalism.[91,92] In previous work,[19] we found that the molar volume of hydrated electrons simulated with DFT was much smaller than that determined experimentally (see also Table 2).[16,19] The partial molar volume for the DC-PBEh hydrated electron is within the uncertainty the same as that of the non-DC PBEh hydrated electron, as also summarized in Table 2. Compared to the experimental value of 26 ± 6 cm^3/mol,[62,63] our DC-DFT simulations using PBEh with 25% and 40% HF exchange both yield significantly underestimated volumes of 5.5 and 9.0 cm^3/mol, respectively. This suggests that even though density correction reduces DDEs, DC-DFT simulations are still not able to correctly capture the solvation structure of the hydrated electron.

The use of DC also enhances the angular ordering of the water molecules around the electron, as shown in Figure 2g,h. This figure shows the distribution of normalized dot products between the water dipole vector and a vector from the center of the electron to the first-shell water oxygen. We chose this measure to better compare to that presented in previous work;[16,35] in the Supporting Information, we also show distributions of coordination angles of the dot product of the O−H bond and the electron-to-oxygen vectors. By both orientational measures, density correction produces a tighter angular orientation of the first-shell waters relative to simulations without DC. This suggests that the hydrated electron in DC-DFT simulations is more kosmotropic than that simulated without density correction. This result is likely at odds with the fact that the experimental solvation entropy of the hydrated electron is large and positive, which indicates that the hydrated electron is a champion chaotrope.[93,94] We previously noted on the basis of ion pairing that the DFT-simulated hydrated electrons are more kosmotropic than Na^+ cations,[35] and we also have shown that the PBEh(25%)-D3 hydrated electron has a negative entropy of solvation.[33] Thus, DC likely brings the solvation entropy of the DFT-simulated hydrated electron farther from the experiment.

We next investigate the electronic absorption spectra of DFT-simulated hydrated electrons simulated with and without DC. Several computational approaches exist for calculating hydrated electron UV−vis spectra, including periodic Tamm−Dancoff Approximation (TDA) time-dependent DFT (TD-DFT) and nonperiodic TD-DFT methods.[89] We argued in previous work[16] that periodic TDA TD-DFT-based spectral calculations lead to overly blue-shifted absorption maxima, which for PBEh(25% and 40%) were approximately 3.0 and 4.4 eV, respectively, compared to the experimental value of 1.7 eV.[66,90] Instead, we showed[16] that nonperiodic TD-DFT[95] with LRC-ωPBE and $\omega = 0.175$ a_0^{-1}, inspired by the work of Uhlig et al.[89] and used in our previous work,[16,38] provides a better approach that reduces finite size effects and provides more reliable VBEs and absorption maxima.[16,89] We show in the Supporting Information that this value of ω satisfies Janak's theorem for PBEh(25% and 40%)-D3 and DC-PBEh(25% and 40%)-D3. Thus, our spectroscopic calculations use the nonperiodic methodology outlined by Uhlig et al.,[89] with uncorrelated configurations from both our standard PBEh and our DC-PBEh trajectories to assess the impact of density correction on electronic transitions.

As demonstrated in previous work[16,96] as well as in Figure 3, simulations of the hydrated electron using PBEh functionals with 25% (red curve) and 40% (orange curve) Hartree−Fock exchange predict absorption spectra with a pronounced (hundreds of meV) blue shift compared to the experimental peak (black curve) near 1.7 eV. Introducing DC (blue and teal curves) does not significantly alter this blue shift; however, both the DC-PBEh(40%) and PBEh(40%) spectra exhibit an unphysical low-energy shoulder, resulting in poorer agreement with experiment. In the Supporting Information, we show that the character of the TD-DFT excited states is unchanged between the 25% and 40% functionals, but that the first few excitations for (DC-)PBEh(40%)-D3 are red-shifted compared to (DC-)PBEh(25%)-D3. We also present an analysis in the Supporting Information of the electrostatic potential in different regions surrounding the electron and show that

https://doi.org/10.1021/acs.jctc.5c01944
J. Chem. Theory Comput. 2026, 22, 2550−2561

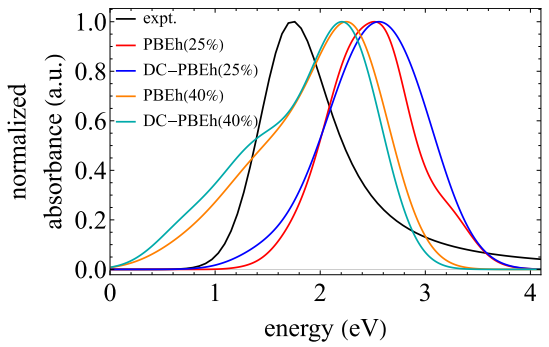

Figure 3. Absorption spectra of the hydrated electron, calculated using nonperiodic TD-DFT with the LRC-ωPBE DFA,[89] from uncorrelated equilibrated configurations extracted from (DC-)DFT trajectories employing different levels of theory. The experimental absorption spectrum is shown as the black curve from refs 66 and 90. For all the DFT-simulated spectra, a blue shift relative to the experimental peak position is observed, with the largest shifts occurring for PBEh(25%) (red) and DC-PBEh(25%) (blue). Increasing the amount of HF exchange slightly decreases the blue-shift in the absorption peak as seen in both PBEh(40%) (orange) and DC-PBEh(40%) (teal).

PBEh(40%)-D3 sees more regions that are electrostatically stable in the bulk outside the central cavity. This extra electrostatic stability of the bulk regions in the water structure is what induces the red shoulder in the (DC-)PBEh(40%)-D3 spectrum.

As mentioned above, PBEh(25%)-D3 and PBEh(40%)-D3 yield similar R_g values of around 2.3 Å, whereas DC-PBEh(25%)-D3 and DC-PBEh(40%)-D3 produce smaller R_g values near 2.0 Å, indicating increased electron localization. The smaller R_g means that one would expect the DC-calculated spectra to be blue-shifted relative to their PBEh-only counterparts, which is not what we observe. To understand this, we also calculated the radius of gyration directly from the nonperiodic TD-DFT calculations with the LRC-ωPBE functional, as described in more detail in the Supporting Information. We find hydrated electron radii of gyration of 2.29 ± 0.1 and 2.8 ± 0.4 for configurations generated from DC-PBEh(25%)-D3 and DC-PBEh(40%)-D3, respectively. These values for the radius of gyration, which are different because of the higher electrostatic attraction in the bulk when (DC-)PBEh(40%)-D3 is used, are indeed consistent with the observed spectroscopic trends. We have previously highlighted similar instances where LRC-ωPBE gives a notably different R_g than the functional used to generate the configurations.[16] Although this disagreement does not occur when the functional used to generate the configurations is also used to calculate TD-DFT excited states, it is well-known that DFAs that are not long-range corrected produce unphysical states that further worsen the agreement of the calculated spectrum with experiment.[16,89]

The fourth column in Table 2 shows that PBEh-based DFT with and without DC substantially underestimates the experimental hydrated electron VBE of 3.5 eV: here, the VBE values were extracted from our nonperiodic LRC-ωPBE TD-DFT calculations to avoid the considerable corrections needed to estimate VBE's from periodic simulations.[78] We note that although VBE values are often extrapolated to infinite system size, as we did in our previous work with the PBE0-D3 functional,[38] here we choose to present the VBEs computed only from our 64 water simulations. Although this makes it difficult to directly compare these values to experiment, our calculations do allow for a direct comparison between different functionals at this system size.

We find that PBEh(25%)-D3 yields an average VBE of 2.14 ± 0.36 eV, while PBEh(40%)-D3 yields 1.78 ± 0.26 eV. Evidently, even though a larger fraction of exact exchange correlates with a red-shift in the computed DFA absorption spectrum, it does not improve agreement with the ∼3.5 eV experimental detachment energy. Applying DC further reduces the predicted VBEs, with DC-PBEh(25%)-D3 and DC-PBEh(40%)-D3 giving 1.76 ± 0.21 eV and 1.70 ± 0.40 eV, respectively. This is somewhat surprising given that DC strongly increased the binding energy of an electron to the idealized Kevan structure, as mentioned above. These results demonstrate that addressing density-driven delocalization worsens experimental agreement, implying that DDEs are not the primary source of VBE error and that the discrepancies with respect to experiment stem from fundamental functional limitations. It is also possible that reducing DDEs with DC worsens any fortuitous cancellation of errors present when the PBEh functional is applied to this system, as we discuss further below.

The Degree of DDEs for DC-DFT-Simulated Hydrated Electrons

To probe the impact of DC on DFT predictions for hydrated electrons in more depth, we carried out the same sensitivity analysis used above but replaced the idealized Kevan structure with instantaneous MD snapshots of the electron's first hydration shell. For each functional, we evaluated a total of five uncorrelated configurations: each of which contained between 4 and 5 water molecules, which are representative of the bulk. The average density sensitivity metrics (eq 2) computed from these MD-derived geometries are given in the right-most column of Table 1, with the full set of data shown in the Supporting Information.

Given that the sensitivity values for configurations extracted from our DC trajectories are well above the 2 kcal/mol threshold, we constructed average $E(N)$ curves for the snapshot water clusters; the error bars reflect both limited statistics and trajectory fluctuations. Notably, increasing HF exchange from 25% to 40% increases the density sensitivity in both sets of snapshots and the Kevan structure. Figure 4a demonstrates that PBEh(40%)-D3 (orange curve) reduces the spurious minimum at fractional charge values observed in PBEh(25%)-D3 (red curve) and is closer to the ideal linear behavior but is still convex, indicative of DDEs. This improvement with an increased percentage of HF exchange is accompanied by an increased cluster electron affinity of over ∼100 meV. However, analysis of Mulliken charges on the sulfur atom of the combined system (Table 1, first shell column) reveals persistent DDEs, with the sulfur atom bearing less than −1 e with both PBEh functionals.

Analysis of snapshots from our DC-PBEh(25% and 40%)-D3, trajectories, represented by navy and purple curves, respectively, in Figure 4b reveals distinct $E(N)$ behavior compared to the uncorrected functionals. The average $E(N)$ curves for the DC functionals are concave, indicating that DDEs are reduced even for the asymmetric snapshots sampled in MD. We also show in Supporting Information that the charging curves exhibit the same qualitative shape when all waters are included, rather than extracting first-shell config-

https://doi.org/10.1021/acs.jctc.5c01944
J. Chem. Theory Comput. 2026, 22, 2550−2561

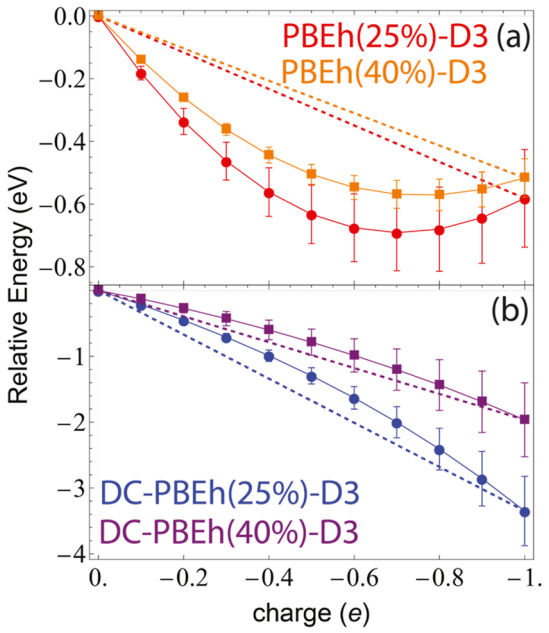

Figure 4. (a,b) $E(N)$ charging plots for Kevan-like DFT-simulated hydrated electron structures derived from the first solvation shells of uncorrelated configurations sampled from PBEh-D3 (a) and DC-PBEh (b) molecular dynamics trajectories. Increasing HF exchange in PBEh-D3 from 25% to 40% reduces the spurious minimum at fractional electron occupation, indicating an improved description of charge localization in the first solvation shell. The application of the DC procedure eliminates the convexity of the charging curves, enhancing charge localization for both the PBEh(25% and 40%)-D3 DFAs. Increasing the HF fraction of the PBEh functional slightly raises the electron affinity of the Kevan structure, while the use of DC increases the model Kevan structure electron affinity by over 2 eV (compare panels a and b). This same behavior is seen in panels a and b of Figure 1.

urations. This makes physical sense as the region binding the excess electron should be by far the most density sensitive, while the neutral bulk waters should not be impacted as much by reducing density-driven errors. As with the model Kevan structure above, the DC $E(N)$ plots show stronger electron binding of the water clusters compared to the standard PBEh-D3 functionals, even though this binding is not reflected in the VBE when calculated nonperiodically with the LRC-ωPBE functional. This suggests that the energy differences are innate to the functionals and not due to differences in the atomic configurations generated by each functional. We also see that for the combined system, the electron is completely localized on the S atom relative to configurations taken from trajectories for both DC functionals, as summarized in Table 1 (first-shell column). All of this confirms the internal consistency of the density correction approach and demonstrates that density correction does effectively address DDEs for DFT-simulated hydrated electrons.

We note that the variations seen between our different MD snapshots are a fundamental aspect of the hydrated electron that is not properly captured by simple structural models. Unlike the idealized Kevan structure, with its octahedrally symmetric arrangement of six waters, real DFT-simulated hydrated electrons exhibit dynamic solvation environments with fluctuating solvation motifs and water coordination numbers ranging from 4 to 5 waters. Each configuration represents a distinct electronic environment where the balance between electron localization and delocalization can vary based on the instantaneous arrangement of the surrounding waters. This statistical perspective reveals why density functionals face particular challenges in predicting experimental observables for hydrated electrons. The excess electron's wave function extends well beyond the first solvation shell, so even small reorientation of more distant waters can alter the electron's energetics and amplify sensitivity to density-driven errors. The DC framework clearly reduces density-driven contributions, but residual functional errors clearly remain, as evidenced by the even poorer agreement with experiment, suggesting a worsening of cancellation of errors at play.

DFT Energy Error Decomposition for the Hydrated Electron

Given that DC decreases the DDEs present in the non-DC MD simulations, we turn next to attempting to quantify whether DC actually worsens intrinsic DFT error cancellations when simulating hydrated electrons. To address this, we use an energy decomposition framework to directly attribute functional-dominant (ΔE_{F}) and density-driven (ΔE_{DDE}) contributions to the total error (ΔE_{tot})[53,97]

$$\Delta E_{\mathrm{tot}} = (\tilde{E}[\tilde{\rho}] - \tilde{E}[\rho]) + (\tilde{E}[\tilde{\rho}] - E[\rho]) \tag{2}$$

$$= \Delta E_{\mathrm{DDE}} + \Delta E_{\mathrm{F}} \tag{3}$$

where $\tilde{E}$ is an approximate energy functional, E is the exact energy functional, $\tilde{\rho}$ is an approximate density, and ρ is the exact density. Of course, rigorously evaluating some of these terms is not feasible, because we do not have access to the exact energy functional and density. Here, we use the LRC-ωPBE energy functional and density as a proxy for the exact energy functional and density. We made this choice based on the fact that LRC-ωPBE shows the most linear charging curve in Figure 1. This then allows the density-driven error for a DC functional to be calculated as[97]

$$\Delta E_{\mathrm{DDE}}(\mathrm{DFA@HF}) = \tilde{E}[\rho_{\mathrm{HF}}] - \tilde{E}[\rho] \tag{4}$$

We note that the density error calculated using eq 4 is really a density-driven energy difference rather than a true density-driven error, as we make no direct comparison with the DFA self-consistent density.[97] Importantly, fortuitous cancellation of errors can bias the apparent ΔE_{tot} if ΔE_{F} and ΔE_{DDE} are of similar magnitudes with opposite signs. To better understand cases where this occurs, we follow previous work that has suggested using the total absolute error (ΔE_{TA}), which sums the absolute values of each term

$$\Delta E_{\mathrm{TA}} = |\Delta E_{\mathrm{DDE}}| + |\Delta E_{\mathrm{F}}| \tag{5}$$

To understand the errors for DFT-simulated hydrated electron systems (relative to LRC-ωPBE), we used eqs 3−5 to calculate each of these energy errors for both the Kevan structure and first-shell configurations sampled from (DC-)PBEh(25%)-D3 MD simulations, with the results summarized in Figure 5; the upper panel shows results for the Kevan structure, while the lower panel shows the results for first-shell configurations extracted from DFT hydrated electron simulations. The Kevan structure and first-shell configurations both show the same clear trend: using the HF density (as in DC, blue bars) actually increases the density error, ΔE_{DDE}, relative to the SC density (orange bars). Moreover, the sign of the density-driven error goes from being negative for the non-DC functionals to being positive with DC.

https://doi.org/10.1021/acs.jctc.5c01944
J. Chem. Theory Comput. 2026, 22, 2550−2561

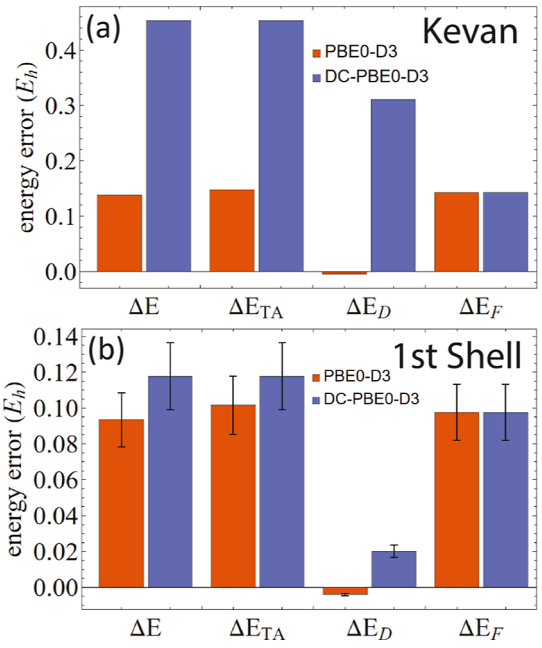

Figure 5. Energy error (ΔE_{tot}), total absolute energy error (ΔE_{TA}), density-driven error (ΔE_D), and functional dominant error (ΔE_F) for the Kevan structure (panel a) and uncorrelated first-shell configurations sampled from a PBEh(25%)-D3 trajectory (panel b) calculated using the LRC-ωPBE functional as the reference ("exact") energy functional and density. The orange bars are the PBEh(25%)-D3 functional and the blue bars are DC-PBEh(25%)-D3. For both the Kevan structure and first-shell configurations, the HF density is overlocalized, leading to increased (and positive) density-driven error for DC. This worsens both the total energy error (ΔE_{tot}) and total absolute energy error (ΔE_{TA}) due to both a worsening of cancellation of errors and an increase in the absolute magnitude of the density-driven error, respectively.

Although this result at first appears to be at odds with Figure 1, which showed that DC qualitatively decreases density errors, it is known that the HF density is overlocalized. PBEh-D3 shows a slightly negative density error (relative to LRC-ωPBE), meaning that the self-consistent PBEh-D3 density is slightly more delocalized than the LRC-ωPBE density. The DC-PBEh-D3 density error is positive and increased in magnitude relative to PBEh-D3 because the HF density is overlocalized compared to the LRC-ωPBE density. Since the functional-dominant error is positive, this indeed constitutes removal of a fortuitous cancellation of errors as well as the increase in the magnitude of the density-driven error. This explains why both the DC total and total absolute errors increase relative to the non-DC functional: the overlocalization of the HF density is "worse" than the excess delocalization present in the SC density.

CONCLUSIONS

Given the tendency of DFAs to exhibit charge delocalization error,[16] we anticipated that evaluating HF densities with DFAs through DC would minimize density-driven errors and yield results more consistent with experimental observations. After confirming the density sensitivity of our DFT-based hydrated electron system, we found that DC indeed successfully reduced charge delocalization arising from DDEs in the combined system, where DC was able to correctly localize the excess electron on the sulfur atom.

Although this approach can address charge delocalization errors, the application of DC to PBEh-D3 functionals also induces worrisome structural and electronic changes in the DFT-simulated hydrated electron system. DC redistributes electron density from the long-distance tails of the charge distribution into the excess electron's cavity, resulting in a decreased radius of gyration and a generally tighter solvation structure. These modifications lead to predicted properties that deviate further from experimental observables compared with the uncorrected PBEh-D3 functionals. This finding elucidates a critical limitation: successfully correcting density-driven errors and reducing charge delocalization does not guarantee improved agreement with experimental measurements. Indeed, DC-PBEh(25% and 40%)-D3 yields poorer agreement with experimental values than standard PBEh(25% and 40%)-D3 functionals, demonstrating that the pursuit of correctness in charge localization may inadvertently compromise a hidden cancellation of errors and thus worsen the accuracy of the computed properties.

The DC framework has demonstrated great success in addressing density-driven errors across numerous chemical systems.[53,55] However, our results suggest that hydrated electron systems may represent a particularly challenging case, where the relationship between charge localization and experimental accuracy is more complex than anticipated. Since hydrated electrons reside primarily between water molecules, we speculate that the errors that an approximate DFA can make on this system depend on: (1) the localization/density-driven error behavior of the functional; (2) the water band gap predicted by the functional, since this dictates how easily the density can donate into the LUMO of nearby waters; and (3) the behavior of the water predicted by the functional, as this impacts coordination of the electron and how much water can penetrate into the charge density. For example, changing the percent of HF exchange changes both the localization of excess charge density as well as the band gap of water, which can cause unexpected results.[18,98] All of these effects are present to some degree for all aqueous anionic systems; however, we expect them to be particularly impactful for hydrated electrons.

Overall, the fact that reducing DDEs makes the agreement with experiment worse strongly indicates that there is a significant inherent error attributed to the DFAs used for modeling this system. We also note that all of the analyses presented here probe the global curvature of $E(N)$. It is also possible to investigate local curvature,[99] which may have implications for how charge is partitioned in the electron cavity versus on nearby solvent molecules, a feature we will investigate in future work.

METHODS

To simulate hydrated electron trajectories with DC-DFT, we used the CP2K[100] software package. Following our previous work,[16,38] we used a simulation cell with 64 water molecules and a single excess electron. Briefly, the PBEh(25% and 40% HF exchange) DFAs, with and without DC, were used with Grimme's D3 dispersion correction,[71] and HF calculations were expedited with the ADMM method using a cFIT3 basis.[101] The temperature was held constant at 298 K via a Nose−Hoover thermostat and a time-step of 0.5 fs was employed.[102] To add density correction to our simulations, we used the energy correction framework in CP2K[100] as presented previously by Belleflamme and Hutter.[103] Single-point energy and Mulliken charge calculations were done in QChem.[104] See Supporting Information for representative input files and trajectory XYZ files.

https://doi.org/10.1021/acs.jctc.5c01944
J. Chem. Theory Comput. 2026, 22, 2550−2561

All $E(N)$ plots were computed by doing explicit fractional charge calculations using the "FRACTIONAL_ELECTRON" keyword in the QChem[104] software package. The LRC-ωPBE calculations for charging curves used an ω value of 0.40 a_0^{-1}. For the Kevan and first-shell charging calculations, the aug-cc-pVTZ basis set was used for all atoms and a ghost atom with a aug-cc-pVQZ basis was placed at the center of the water cavity. D3 dispersion corrections[71] were used for all charging curve calculations for both the PBEh and DC-PBEh functionals. The calculation of the radius of gyration and charge distributions was done with in-house Python scripts and computed using the spin density, while the angular distributions were computed with a Mathematica script. Radial distribution functions were calculated in VMD.

Nonperiodic TD-DFT spectroscopy calculations were done in QChem[104] using the LRC-ωPBE functional with an ω value of 0.175 a_0^{-1} and a 6-31++G* basis set. Previously, we have found that this value is optimal for satisfying Janak's theorem for this system simulated with the PBEh(25%) functional.[38] In the Supporting Information, we show that this same ω value also satisfies Janak's theorem for PBEh(40%)-D3 and DC-PBEh(25% and 40%)-D3. Instantaneous MD snapshots were sampled every picosecond from our simulations, which as shown in the Supporting Information provides configurations that are uncorrelated. For each snapshot, in addition to the 64 quantum mechanical waters surrounding the electron center of mass, we replicated the simulation box 26 times with point charges at the positions of the atoms of each water molecule. This was done to prevent the spilling of electron density out of the central quantum mechanical box. In the Supporting Information, we also investigate the quantum mechanical region size dependence on the spectra and show that it is not sensitive to the number of QM waters.

■ ASSOCIATED CONTENT

Data Availability Statement

Additional data for reproducing the results of this manuscript can be found in a persistent online repository (10.5061/dryad.80gb5mm32). This repository also includes representative input files for running the calculations outlined in the Methods section.

Supporting Information

The Supporting Information is available free of charge at https://pubs.acs.org/doi/10.1021/acs.jctc.5c01944.

Further description of the methods and simulation parameters used in this work, as well as discussion on the use of an alternate interpolation method for computing $E(N)$ charging curves (PDF)

■ AUTHOR INFORMATION

Corresponding Author

Benjamin J. Schwartz − *Department of Chemistry & Biochemistry, University of California, Los Angeles, Los Angeles, California 90095-1569, United States;* orcid.org/0000-0003-3257-9152; Phone: (310) 206-4113; Email: schwartz@chem.ucla.edu

Authors

William R. Borrelli − *Department of Chemistry & Biochemistry, University of California, Los Angeles, Los Angeles, California 90095-1569, United States*

José L. Guardado Sandoval − *Department of Chemistry & Biochemistry, University of California, Los Angeles, Los Angeles, California 90095-1569, United States*

Complete contact information is available at: https://pubs.acs.org/10.1021/acs.jctc.5c01944

Notes

The authors declare no competing financial interest.

■ ACKNOWLEDGMENTS

This work was supported by the National Science Foundation under grant CHE-2247583. Partial support for W.R.B. came from the US Department of Energy, CPIMS under grant DE-SC0017800. Computational resources were provided by the UCLA Institute for Digital Research and Education as well as the Expanse computing cluster at the San Diego Supercomputer Center through allocation CHE240203 from the Advanced Cyberinfrastructure Coordination Ecosystem: Services & Support (ACCESS) program, which is supported by the U.S. National Science Foundation grants 2138259, 2138286, 2138307, 2137603, and 2138296.

■ REFERENCES

(1) Garrett, B. C.; et al. Role of Water in Electron-Initiated Processes and Radical Chemistry: Issues and Scientific Advances. *Chem. Rev.* **2005**, *105*, 355−390.

(2) Jonah, C. D. A. Short History of the Radiation Chemistry of Water. *Radiat. Res.* **1995**, *144*, 141−147.

(3) Sopena Moros, A.; Li, S.; Li, K.; Doumy, G.; Southworth, S. H.; Otolski, C.; Schaller, R. D.; Kumagai, Y.; Rubensson, J. E.; Simon, M.; et al. Tracking Cavity Formation in Electron Solvation: Insights from X-ray Spectroscopy and Theory. *J. Am. Chem. Soc.* **2024**, *146*, 3262−3269.

(4) Marin, T. W.; Jonah, C. D.; Bartels, D. M. Reaction of OH* radicals with H2 in sub-critical water. *Chem. Phys. Lett.* **2003**, *371*, 144−149.

(5) Hart, E. J. The Hydrated Electron. *Science* **1964**, *146*, 19−25.

(6) Gordon, S.; Hart, E. J.; Matheson, M. S.; Rabani, J.; Thomas, J. K. Reactions of the hydrated electron. *Discuss. Faraday Soc.* **1963**, *36*, 193−205.

(7) Gao, X.-F.; Hood, D.; Nathanson, G. M. Deducing Reaction and Diffusion Depths of Near-Interfacial Solvated Electrons from pH-Dependent Product Evaporation. *J. Phys. Chem. B* **2025**, *129*, 1795−1804.

(8) Jordan, C. J. C.; Coons, M. P.; Herbert, J. M.; Verlet, J. R. R. Spectroscopy and dynamics of the hydrated electron at the water/air interface. *Nat. Commun.* **2024**, *15*, 182.

(9) Sagar, D. M.; Bain, C. D.; Verlet, J. R. R. Hydrated Electrons at the Water/Air Interface. *J. Am. Chem. Soc.* **2010**, *132*, 6917−6919.

(10) Uhlig, F.; Marsalek, O.; Jungwirth, P. Electron at the Surface of Water: Dehydrated or Not? *J. Phys. Chem. Lett.* **2013**, *4*, 338−343.

(11) Madarász, A.; Rossky, P. J.; Turi, L. Excess electron relaxation dynamics at water/air interfaces. *J. Chem. Phys.* **2007**, *126*, 234707.

(12) Alizadeh, E.; Sanche, L. Precursors of Solvated Electrons in Radiobiological Physics and Chemistry. *Chem. Rev.* **2012**, *112*, 5578−5602.

(13) Westphal, K.; Wiczk, J.; Miloch, J.; Kciuk, G.; Bobrowski, K.; Rak, J. Irreversible electron attachment − a key to DNA damage by solvated electrons in aqueous solution. *Org. Biomol. Chem.* **2015**, *13*, 10362−10369.

(14) Rezaee, M.; Sanche, L.; Hunting, D. J. Cisplatin Enhances the Formation of DNA Single- and Double-Strand Breaks by Hydrated Electrons and Hydroxyl Radicals. *Radiat. Res.* **2013**, *179*, 323−331.

(15) Herbert, J. M.; Coons, M. P. The Hydrated Electron. *Annu. Rev. Phys. Chem.* **2017**, *68*, 447−472.

(16) Borrelli, W. R.; Liu, X.; Schwartz, B. J. How the choice of exchange−correlation functional affects DFT-based simulations of the hydrated electron. *J. Chem. Phys.* **2025**, *162*, 110901.

(17) Tauber, M. J.; Mathies, R. A. Structure of the Aqueous Solvated Electron from Resonance Raman Spectroscopy: Lessons from Isotopic Mixtures. *J. Am. Chem. Soc.* **2003**, *125*, 1394−1402.

(18) Borrelli, W. R.; Liu, X.; Schwartz, B. J. Evaluating the Chemical Reactivity of DFT-Simulated Liquid Water with Hydrated Electrons

via the Dual Descriptor. *J. Chem. Theory Comput.* **2024**, *20*, 9571−9579.
(19) Borrelli, W. R.; Mei, K. J.; Park, S. J.; Schwartz, B. J. Partial Molar Solvation Volume of the Hydrated Electron Simulated Via DFT. *J. Phys. Chem. B* **2024**, *128*, 2425−2431.
(20) Neupane, P.; Bartels, D. M.; Thompson, W. H. Exploring the Unusual Reactivity of the Hydrated Electron with CO2. *J. Phys. Chem. B* **2024**, *128*, 567−575.
(21) Neupane, P.; Bartels, D. M.; Thompson, W. H. Empirically Optimized One-Electron Pseudopotential for the Hydrated Electron: A Proof-of-Concept Study. *J. Phys. Chem. B* **2023**, *127*, 7361−7371.
(22) Tay, K. A.; Coudert, F.-X.; Boutin, A. Mechanism and kinetics of hydrated electron diffusion. *J. Chem. Phys.* **2008**, *129*, 054505.
(23) Tay, K. A.; Boutin, A. Hydrated Electron Diffusion: The Importance of Hydrogen-Bond Dynamics. *J. Phys. Chem. B* **2009**, *113*, 11943−11949.
(24) Nicolas, C.; Boutin, A.; Lévy, B.; Borgis, D. Molecular simulation of a hydrated electron at different thermodynamic state points. *J. Chem. Phys.* **2003**, *118*, 9689−9696.
(25) Schnitker, J.; Rossky, P. J. An electron−water pseudopotential for condensed phase simulation. *J. Chem. Phys.* **1987**, *86*, 3462−3470.
(26) Turi, L.; Borgis, D. Analytical investigations of an electron−water molecule pseudopotential. II. Development of a new pair potential and molecular dynamics simulations. *J. Chem. Phys.* **2002**, *117*, 6186−6195.
(27) Glover, W. J.; Schwartz, B. J. Short-Range Electron Correlation Stabilizes Noncavity Solvation of the Hydrated Electron. *J. Chem. Theory Comput.* **2016**, *12*, 5117−5131.
(28) Larsen, R. E.; Glover, W. J.; Schwartz, B. J. Does the Hydrated Electron Occupy a Cavity? *Science* **2010**, *329*, 65−69.
(29) Glover, W. J.; Schwartz, B. J. The Fluxional Nature of the Hydrated Electron: Energy and Entropy Contributions to Aqueous Electron Free Energies. *J. Chem. Theory Comput.* **2020**, *16*, 1263−1270.
(30) Turi, L.; Rossky, P. J. Theoretical Studies of Spectroscopy and Dynamics of Hydrated Electrons. *Chem. Rev.* **2012**, *112*, 5641−5674.
(31) Ahmadi, S. Hydrated electrons and cluster science. *J. Mol. Struct.* **2022**, *1250*, 131898.
(32) Neupane, P.; Bartels, D. M.; Thompson, W. H. Relation between the Hydrated Electron Solvation Structure and Its Partial Molar Volume. *J. Phys. Chem. B* **2023**, *127*, 5941.
(33) Borrelli, W. R.; Liu, X.; Schwartz, B. J. The Solvation Entropy of Different Simulation Models of the Hydrated Electron. *J. Phys. Chem. Lett.* **2026**, *17*, 1899−1906.
(34) Zho, C.-C.; Farr, E. P.; Glover, W. J.; Schwartz, B. J. Temperature dependence of the hydrated electron's excited-state relaxation. I. Simulation predictions of resonance Raman and pump-probe transient absorption spectra of cavity and non-cavity models. *J. Chem. Phys.* **2017**, *147*, 074503.
(35) Park, S. J.; Narvaez, W. A.; Schwartz, B. J. Ab Initio Studies of Hydrated Electron/Cation Contact Pairs: Hydrated Electrons Simulated with Density Functional Theory Are Too Kosmotropic. *J. Phys. Chem. Lett.* **2023**, *14*, 559−566.
(36) Pizzochero, M.; Ambrosio, F.; Pasquarello, A. Picture of the wet electron: a localized transient state in liquid water. *Chem. Sci.* **2019**, *10*, 7442−7448.
(37) Mei, K. J.; Borrelli, W. R.; Guardado Sandoval, J. L.; Schwartz, B. J. How to Probe Hydrated Dielectrons Experimentally: Ab Initio Simulations of the Absorption Spectra of Aqueous Dielectrons, Electron Pairs, and Hydride. *J. Phys. Chem. Lett.* **2024**, *15*, 9557−9565.
(38) Park, S. J.; Schwartz, B. J. Understanding the Temperature Dependence and Finite Size Effects in Ab Initio MD Simulations of the Hydrated Electron. *J. Chem. Theory Comput.* **2022**, *18*, 4973−4982.
(39) Herbert, J. M.; Head-Gordon, M. Calculation of Electron Detachment Energies for Water Cluster Anions: An Appraisal of Electronic Structure Methods, with Application to (H2O)20- and (H2O)24-. *J. Phys. Chem. A* **2005**, *109*, 5217−5229.
(40) Kumar, A.; Walker, J. A.; Bartels, D. M.; Sevilla, M. D. A Simple ab Initio Model for the Hydrated Electron That Matches Experiment. *J. Phys. Chem. A* **2015**, *119*, 9148−9159.
(41) Park, S. J.; Schwartz, B. J. Evaluating Simple Ab Initio Models of the Hydrated Electron: The Role of Dynamical Fluctuations. *J. Phys. Chem. B* **2020**, *124*, 9592−9603.
(42) Gao, L.; Zhang, L.; Fu, Q.; Bu, Y. Molecular Dynamics Characterization of Dielectron Hydration in Liquid Water with Unique Double Proton Transfers. *J. Chem. Theory Comput.* **2021**, *17*, 666−677.
(43) Barnett, R. N.; Giniger, R.; Cheshnovsky, O.; Landman, U. Dielectron Attachment and Hydrogen Evolution Reaction in Water Clusters. *J. Phys. Chem. A* **2011**, *115*, 7378−7391.
(44) Borrelli, W. R.; Sandoval, J. L. G.; Mei, K. J.; Schwartz, B. J. Roles of H-Bonding and Hydride Solvation in the Reaction of Hydrated (Di)electrons with Water to Create H2 and OH. *J. Chem. Theory Comput.* **2024**, *20*, 7337−7346.
(45) Gillan, M. J.; Alfè, D.; Michaelides, A. Perspective: How good is DFT for water? *J. Chem. Phys.* **2016**, *144*, 130901.
(46) Lin, I.-C.; Seitsonen, A. P.; Coutinho-Neto, M. D.; Tavernelli, I.; Rothlisberger, U. Importance of van der Waals Interactions in Liquid Water. *J. Phys. Chem. B* **2009**, *113*, 1127−1131.
(47) Chen, M.; Ko, H.-Y.; Remsing, R. C.; Calegari Andrade, M. F.; Santra, B.; Sun, Z.; Selloni, A.; Car, R.; Klein, M. L.; Perdew, J. P.; Wu, X. Ab initio theory and modeling of water. *Proc. Natl. Acad. Sci. U.S.A.* **2017**, *114*, 10846−10851.
(48) Gaiduk, A. P.; Gygi, F.; Galli, G. Density and Compressibility of Liquid Water and Ice from First-Principles Simulations with Hybrid Functionals. *J. Phys. Chem. Lett.* **2015**, *6*, 2902−2908.
(49) Uhlig, F. Structure, dynamics and reactivity of the hydrated electron, Ph.D. thesis, Academy of Sciences of the Czech Republic, 2014.
(50) Casey, J. R.; Kahros, A.; Schwartz, B. J. To Be or Not to Be in a Cavity: The Hydrated Electron Dilemma. *J. Phys. Chem. B* **2013**, *117*, 14173−14182.
(51) Uhlig, F.; Marsalek, O.; Jungwirth, P. Unraveling the Complex Nature of the Hydrated Electron. *J. Phys. Chem. Lett.* **2012**, *3*, 3071−3075.
(52) Mori-Sánchez, P.; Cohen, A. J.; Yang, W. Many-electron self-interaction error in approximate density functionals. *J. Chem. Phys.* **2006**, *125*, 201102.
(53) Song, S.; Vuckovic, S.; Sim, E.; Burke, K. Density-Corrected DFT Explained: Questions and Answers. *J. Chem. Theory Comput.* **2022**, *18*, 817−827.
(54) Vuckovic, S.; Song, S.; Kozlowski, J.; Sim, E.; Burke, K. Density Functional Analysis: The Theory of Density-Corrected DFT. *J. Chem. Theory Comput.* **2019**, *15*, 6636−6646.
(55) Sim, E.; Song, S.; Vuckovic, S.; Burke, K. Improving Results by Improving Densities: Density-Corrected Density Functional Theory. *J. Am. Chem. Soc.* **2022**, *144*, 6625−6639.
(56) Sim, E.; Kim, M.-C.; Burke, K. Dissociation curves of diatomic molecules: A DC-DFT study. *AIP Conf. Proc.* **2015**, *1702*, 090036.
(57) Dasgupta, S.; Shahi, C.; Bhetwal, P.; Perdew, J. P.; Paesani, F. How Good Is the Density-Corrected SCAN Functional for Neutral and Ionic Aqueous Systems, and What Is So Right about the Hartree−Fock Density? *J. Chem. Theory Comput.* **2022**, *18*, 4745−4761.
(58) Kim, M.-C.; Sim, E.; Burke, K. Ions in solution: Density corrected density functional theory (DC-DFT). *J. Chem. Phys.* **2014**, *140*, 18A528.
(59) Kim, M.-C.; Park, H.; Son, S.; Sim, E.; Burke, K. Improved DFT Potential Energy Surfaces via Improved Densities. *J. Phys. Chem. Lett.* **2015**, *6*, 3802−3807.
(60) Kim, Y.; Sim, M.; Lee, M.; Kim, S.; Song, S.; Burke, K.; Sim, E. Extending Density-Corrected Density Functional Theory to Large Molecular Systems. *J. Phys. Chem. Lett.* **2025**, *16*, 939−947.
(61) Johnson, E. R.; Otero-de-la Roza, A.; Dale, S. G. Extreme density-driven delocalization error for a model solvated-electron system. *J. Chem. Phys.* **2013**, *139*, 184116.

https://doi.org/10.1021/acs.jctc.5c01944
J. Chem. Theory Comput. 2026, 22, 2550−2561

(62) Janik, I.; Lisovskaya, A.; Bartels, D. M. Partial Molar Volume of the Hydrated Electron. *J. Phys. Chem. Lett.* **2019**, *10*, 2220−2226.
(63) Borsarelli, C. D.; Bertolotti, S. G.; Previtali, C. M. Thermodynamic changes associated with the formation of the hydrated electron after photoionization of inorganic anions: a time-resolved photoacoustic study. *Photochem. Photobiol. Sci.* **2003**, *2*, 791−795.
(64) Shreve, A. T.; Yen, T. A.; Neumark, D. M. Photoelectron spectroscopy of hydrated electrons. *Chem. Phys. Lett.* **2010**, *493*, 216−219.
(65) LaForge, A.; et al. Real-Time Dynamics of the Formation of Hydrated Electrons upon Irradiation of Water Clusters with Extreme Ultraviolet Light. *Phys. Rev. Lett.* **2019**, *122*, 133001.
(66) Jou, F.-Y.; Freeman, G. R. Temperature and isotope effects on the shape of the optical absorption spectrum of solvated electrons in water. *J. Phys. Chem.* **1979**, *83*, 2383−2387.
(67) Bartels, D. M. Moment analysis of hydrated electron cluster spectra: Surface or internal states? *J. Chem. Phys.* **2001**, *115*, 4404−4405.
(68) Hernandez, D. J.; Rettig, A.; Head-Gordon, M. A New View on Density Corrected DFT: Can One Get a Better Answer for a Good Reason? *arXiv* **2023**, arXiv:2306.15016.
(69) Becke, A. D. Density-functional exchange-energy approximation with correct asymptotic behavior. *Phys. Rev. A:At., Mol., Opt. Phys.* **1988**, *38*, 3098−3100.
(70) Lee, C.; Yang, W.; Parr, R. G. Development of the Colle-Salvetti correlation-energy formula into a functional of the electron density. *Phys. Rev. B* **1988**, *37*, 785−789.
(71) Grimme, S.; Antony, J.; Ehrlich, S.; Krieg, H. A consistent and accurate ab initio parametrization of density functional dispersion correction (DFT-D) for the 94 elements H-Pu. *J. Chem. Phys.* **2010**, *132*, 154104.
(72) VandeVondele, J.; Sprik, M. A molecular dynamics study of the hydroxyl radical in solution applying self-interaction-corrected density functional methods. *Phys. Chem. Chem. Phys.* **2005**, *7*, 1363−1367.
(73) Perdew, J. P.; Ernzerhof, M.; Burke, K. Rationale for mixing exact exchange with density functional approximations. *J. Chem. Phys.* **1996**, *105*, 9982−9985.
(74) Vydrov, O. A.; Scuseria, G. E. Assessment of a long-range corrected hybrid functional. *J. Chem. Phys.* **2006**, *125*, 234109.
(75) Kim, Y.; Song, S.; Sim, E.; Burke, K. Halogen and Chalcogen Binding Dominated by Density-Driven Errors. *J. Phys. Chem. Lett.* **2019**, *10*, 295−301.
(76) Janak, J. F. Proof that in density-functional theory. *Phys. Rev. B* **1978**, *18*, 7165−7168.
(77) Li, C.; Yang, W. On the piecewise convex or concave nature of ground state energy as a function of fractional number of electrons for approximate density functionals. *J. Chem. Phys.* **2017**, *146*, 074107.
(78) Ambrosio, F.; Miceli, G.; Pasquarello, A. Electronic levels of excess electrons in liquid water. *J. Phys. Chem. Lett.* **2017**, *8*, 2055−2059.
(79) Dale, S. G.; Johnson, E. R. Counterintuitive electron localisation from density-functional theory with polarisable solvent models. *J. Chem. Phys.* **2015**, *143*, 184112.
(80) Kevan, L. Solvated electron structure in glassy matrixes. *Acc. Chem. Res.* **1981**, *14*, 138−145.
(81) Narvaez, W. A.; Neupane, P.; Bartels, D. M.; Thompson, W. H. Ab Initio Molecular Dynamics Study of the Reduction of Acetone by the Hydrated Electron. *J. Phys. Chem. B* **2025**, *129*, 8201.
(82) Ambrosio, F.; Miceli, G.; Pasquarello, A. Redox levels in aqueous solution: Effect of van der Waals interactions and hybrid functionals. *J. Chem. Phys.* **2015**, *143*, 244508.
(83) Caldeweyher, E.; Ehlert, S.; Hansen, A.; Neugebauer, H.; Spicher, S.; Bannwarth, C.; Grimme, S. A generally applicable atomic-charge dependent London dispersion correction. *J. Chem. Phys.* **2019**, *150*, 154122.
(84) Lee, M.; Kim, B.; Sim, M.; Sogal, M.; Kim, Y.; Yu, H.; Burke, K.; Sim, E. Correcting Dispersion Corrections with Density-Corrected DFT. *J. Chem. Theory Comput.* **2024**, *20*, 7155−7167.
(85) Graf, D.; Thom, A. J. W. Simple and Efficient Route toward Improved Energetics within the Framework of Density-Corrected Density Functional Theory. *J. Chem. Theory Comput.* **2023**, *19*, 5427−5438.
(86) Martín-Fernández, C.; Harvey, J. N. On the Use of Normalized Metrics for Density Sensitivity Analysis in DFT. *J. Phys. Chem. A* **2021**, *125*, 4639−4652.
(87) Kepp, K. P. Energy vs. density on paths toward more exact density functionals. *Phys. Chem. Chem. Phys.* **2018**, *20*, 7538−7548.
(88) Kanungo, B.; Kaplan, A. D.; Shahi, C.; Gavini, V.; Perdew, J. P. Unconventional Error Cancellation Explains the Success of Hartree−Fock Density Functional Theory for Barrier Heights. *J. Phys. Chem. Lett.* **2024**, *15*, 323−328.
(89) Uhlig, F.; Herbert, J. M.; Coons, M. P.; Jungwirth, P. Optical Spectroscopy of the Bulk and Interfacial Hydrated Electron from Ab Initio Calculations. *J. Phys. Chem. A* **2014**, *118*, 7507−7515.
(90) Abel, B.; Buck, U.; Sobolewski, A. L.; Domcke, W. On the nature and signatures of the solvated electron in water. *Phys. Chem. Chem. Phys.* **2012**, *14*, 22−34.
(91) Kirkwood, J. G.; Buff, F. P. The Statistical Mechanical Theory of Solutions. I. *J. Chem. Phys.* **1951**, *19*, 774−777.
(92) Ben-Naim, A. The Kirkwood−Buff integrals for one-component liquids. *J. Chem. Phys.* **2008**, *128*, 234501.
(93) Han, P.; Bartels, D. M. Reevaluation of Arrhenius parameters for hydrogen atom + hydroxide.fwdarw. (e-)aq + water and the enthalpy and entropy of hydrated electrons. *J. Phys. Chem.* **1990**, *94*, 7294−7299.
(94) Han, P.; Bartels, D. M. On the hydrated electron as a structure-breaking ion. *J. Phys. Chem.* **1991**, *95*, 5367−5370.
(95) Runge, E.; Gross, E. K. U. Density-Functional Theory for Time-Dependent Systems. *Phys. Rev. Lett.* **1984**, *52*, 997−1000.
(96) Lan, J.; Rybkin, V. V.; Pasquarello, A. Temperature Dependent Properties of the Aqueous Electron. *Angew. Chem., Int. Ed.* **2022**, *61*, No. e202209398.
(97) Kaplan, A. D.; Shahi, C.; Bhetwal, P.; Sah, R. K.; Perdew, J. P. Understanding Density-Driven Errors for Reaction Barrier Heights. *J. Chem. Theory Comput.* **2023**, *19*, 532−543.
(98) Lambros, E.; Hu, J.; Paesani, F. Assessing the Accuracy of the SCAN Functional for Water through a Many-Body Analysis of the Adiabatic Connection Formula. *J. Chem. Theory Comput.* **2021**, *17*, 3739−3749.
(99) Zhao, Q.; Ioannidis, E. I.; Kulik, H. J. Global and local curvature in density functional theory. *J. Chem. Phys.* **2016**, *145*, 054109.
(100) Kühne, T. D.; et al. CP2K: An electronic structure and molecular dynamics software package - Quickstep: Efficient and accurate electronic structure calculations. *J. Chem. Phys.* **2020**, *152*, 194103.
(101) Guidon, M.; Hutter, J.; VandeVondele, J. Auxiliary Density Matrix Methods for HartreeFock Exchange Calculations. *J. Chem. Theory Comput.* **2010**, *6*, 2348−2364.
(102) Martyna, G. J.; Klein, M. L.; Tuckerman, M. Nosé−Hoover chains: The canonical ensemble via continuous dynamics. *J. Chem. Phys.* **1992**, *97*, 2635−2643.
(103) Belleflamme, F.; Hutter, J. Radicals in aqueous solution: assessment of density-corrected SCAN functional. *Phys. Chem. Chem. Phys.* **2023**, *25*, 20817−20836.
(104) Epifanovsky, E.; Gilbert, A. T. B.; Feng, X.; Lee, J.; Mao, Y.; Mardirossian, N.; Pokhilko, P.; White, A. F.; Coons, M. P.; Dempwolff, A. L.; et al. Software for the frontiers of quantum chemistry: An overview of developments in the Q-Chem 5 package. *J. Chem. Phys.* **2021**, *155*, 084801.

https://doi.org/10.1021/acs.jctc.5c01944
J. Chem. Theory Comput. 2026, 22, 2550−2561